PROCEEDINGS OF SCIENCE

Study of e^+e^- annihilation to hadrons with SND at VEPP-2000

V. P. Druzhinin*[ab], M. N. Achasov[ab], A. Yu. Barnyakov[a], K. I. Beloborodov[ab], A. V. Berdyugin[ab], A. G. Bogdanchikov[a], A. A. Botov[a], T. V. Dimova[ab], L. V. Kardapoltsev[ab], A. G. Kharlamov[ab], A. A. Korol[ab], D. P. Kovrizhin[a], A. S. Kupich[a], N. A. Melnikova[a] A. E. Obrazovsky[a], E. V. Pakhtusova[a], K. V. Pugachev[ab], S. I. Serednyakov[ab], D. A. Shtol[a], Z. K. Silagadze[ab], I. K. Surin[a], Yu. V. Usov[a] and V. N. Zabin[a].

[a] *Budker Institute of Nuclear Physics, Novosibirsk, 630090, Russia*

[b] *Novosibirsk State University, Novosibirsk, 630090, Russia*

E-mail: druzhinin@inp.nsk.su

Recent results on e^+e^- annihilation to hadrons below 2 GeV obtained at the SND experiment at the VEPP-2000 collider are presented. In particular, we discuss measurements of the $e^+e^- \to \pi^+\pi^-$ and $e^+e^- \to n\bar{n}$ cross sections, and study of the processes $e^+e^- \to \pi^+\pi^-\pi^0$, $K^+K^-\pi^0$, $\eta\pi^0\gamma$, and $\eta\eta\gamma$.

*** *The European Physical Society Conference on High Energy Physics (EPS-HEP2021),* ***
** *26-30 July 2021* ***
** *Online conference, jointly organized by UniversitÃd't Hamburg and the research center DESY* ***

*Speaker.

PoS(EPS-HEP2021)404

Table 1: The distribution of the integrated luminosity (IL) recorded by SND at VEPP-2000 over different energy regions.

Energy range (GeV)	0.30–0.97	0.98–1.06	1.06–2.00
IL (pb^{-1})	77	31	259

1. Introduction

SND [1, 2, 3, 4] is the universal nonmagnetic detector consisting of a nine-layer drift chamber, aerogel Cherenkov counters, a three-layer spherical electromagnetic calorimeter with 1640 NaI(Tl) crystals, and a muon system.

SND has been collecting data at the VEPP-2000 e^+e^- collider [5] since 2010 in the energy range 0.3–2.0 GeV. To date, a data sample with an integrated luminosity of about 370 pb^{-1} has been recorded. The distribution of integrated luminosity collected by SND over different energy regions is presented in Table 1.

Main physics task of the SND experiment is the study of all possible processes of e^+e^- annihilation into hadrons below 2 GeV. In particular, these measurements are used to obtain the total hadronic cross section needed for Standard Model calculation of the anomalous magnetic moment of muon and running electromagnetic coupling constant. A detailed study of dynamic of exclusive processes is also performed. In this report we present SND results on the processes $e^+e^- \to \pi^+\pi^-$, $e^+e^- \to n\bar{n}$, $e^+e^- \to \pi^+\pi^-\pi^0$, $e^+e^- \to K^+K^-\pi^0$, $e^+e^- \to \eta\pi^0\gamma$, and $e^+e^- \to \eta\eta\gamma$.

2. Measurement of the $e^+e^- \to \pi^+\pi^-$ cross section

The process $e^+e^- \to \pi^+\pi^-$ is very important for calculation of the hadronic contribution to the $(g-2)$ of muon. There are many measurements of this process, some of them have systematic uncertainty less than 1%.

Our measurement [6] is based on 4.6 pb^{-1} data collected in the energy range 0.53–0.88 GeV, about 10% of the full SND data set in this range. The event selection is based on excellent e/π separation provided by the three layer SND calorimeter [7]. The measured $e^+e^- \to \pi^+\pi^-$ cross section is shown in Fig. 1 (left). The systematic uncertainty in the measurement is 0.8% in the energy range 0.6–0.9 GeV and 0.9% below 0.6 GeV. The curve in Fig. 1 (left) is the result of the fit to the data with the vector-meson-dominance (VMD) model including the $\rho(770)$, $\omega(782)$, and $\rho(1450)$ resonances. The model describes data well, the obtained resonance parameters are in reasonable agreement with the previous SND measurement [8] and the Particle Data Group table [9].

Our measurement of the $e^+e^- \to \pi^+\pi^-$ cross section are in agreement with the previous energy-scan measurements performed at the VEPP-2M collider with the CMD-2 [10] and SND [8] detectors. The comparison of the fit to the SND data with the currently most accurate BABAR [11] and KLOE [12] measurements performed using the initial-state radiation technique is presented in Fig. 1 (middle and right). The systematic difference is observed between the SND and BABAR data below 0.7 GeV and between the SND and KLOE data above 0.7 GeV.

The contribution to the muon anomalous magnetic moment from the $e^+e^- \to \pi^+\pi^-$ channel in the energy region 0.53–0.88 GeV calculated using the new SND data is $(409.8 \pm 1.4 \pm 3.9) \times$

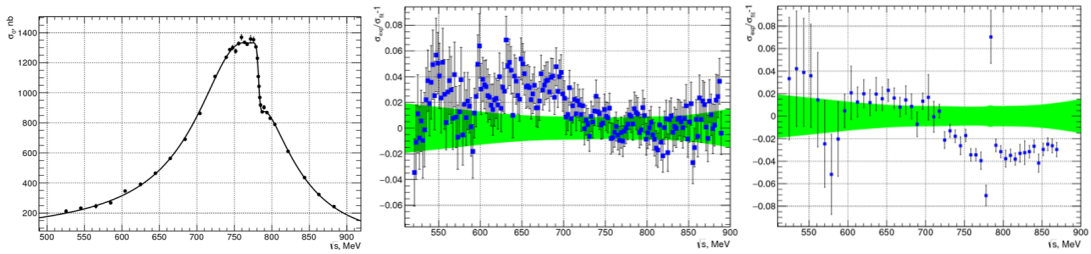

Figure 1: Left panel: The $e^+e^- \to \pi^+\pi^-$ cross section measured by SND. The curve is the result of the VMD fit. The relative difference between the BABAR [11] (middle panel) and KLOE [12] (right panel) $e^+e^- \to \pi^+\pi^-$ data and the SND fit. The band represents the statistical and systematic uncertainties of the SND fit combined in quadrature.

.

10^{-10}. This value is in good agreement with the values obtained using the previous SND [8], BABAR [11], and KLOE [12] data: $(406.5 \pm 1.7 \pm 5.3) \times 10^{-10}$, $(413.6 \pm 2.0 \pm 2.3) \times 10^{-10}$, and $(403.4 \pm 0.7 \pm 2.5) \times 10^{-10}$, respectively.

3. Study of the process $e^+e^- \to n\bar{n}$

The process $e^+e^- \to n\bar{n}$ was previously measured by FENICE [13], and SND [14] using the 2011-2012 data set. The new SND measurement is based on 2017 and 2019 data and uses a different method of signal-background separation compared with Ref. [14].

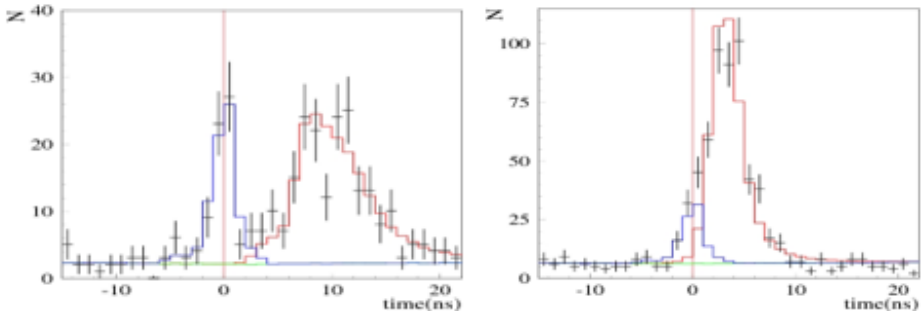

Figure 2: The time distribution for selected data events collected in 2019 (points with error bars) at $E = 1.89$ GeV (left panel) and 1.95 GeV (right panel). The blue histogram is the fitted total contribution of the cosmic-ray, beam-induced and physical backgrounds. The red histogram is the sum of the cosmic-ray background and fitted $n\bar{n}$ signal.

.

For 2017 data, we analyze the distribution of the time difference between the calorimeter trigger and the beam revolution frequency. This difference is measured with a rather poor resolution of about 6 ns. In the 2019 run, the time measurement technique in the calorimeter was significantly improved [15]. For each calorimeter crystal, the signal from the photodetector shaped with an integration time of about 1 μs is digitized by a flash ADC with a sampling rate of 36 MHz. The signal amplitude and its arrival time are determined from the fit to the measured signal shape. The

event time is calculated as a weighted average of crystal arrival times with the energy deposition used as a weight. The time resolution measured using $e^+e^- \to \gamma\gamma$ events is 0.8 ns, nearly an order of magnitude lower than that for the 2017 run.

The time distributions for selected data events of the 2019 run at $E = 1.89$ GeV and 1.95 GeV are shown in Fig. 2. The time distribution consists of the nearly uniform cosmic-ray distribution, the distribution for the beam-induced and physical backgrounds, which is peaked near zero, and a wide $n\bar{n}$ distribution, which is shifted relative to other e^+e^- annihilation events due to small antineutron velocity. From the fit to data with the sum of the three distributions, we determine the number of $n\bar{n}$ events. The shape of the beam-induced and physical background distribution is measured using data recorded below the $n\bar{n}$ threshold.

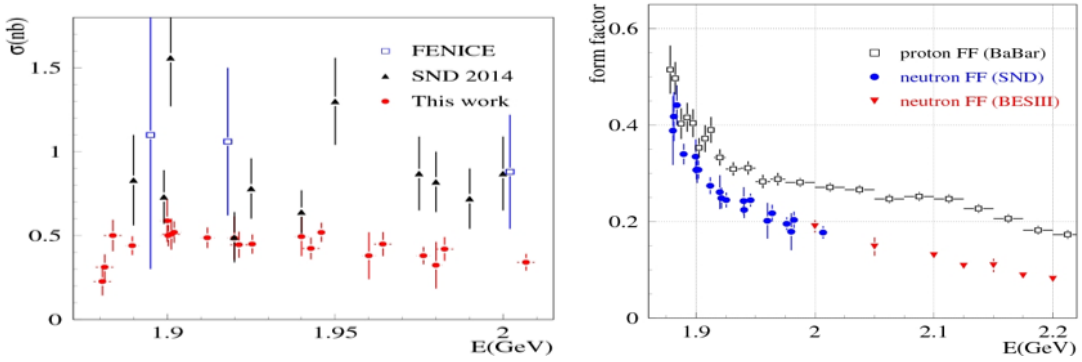

Figure 3: Left panel: The preliminary SND results on the $e^+e^- \to n\bar{n}$ cross section (solid circles) compared with the previous FENICE [13] (empty squares) and SND [14] (filled triangles) measurements. Only statistical error are shown. Right panel: The SND preliminary result on the neutron effective form factor (circles), compared with the BESIII [17] neutron form factor (stars) and the proton form factor measured by BABAR [16] (empty squares).

.

Our preliminary results on the $e^+e^- \to n\bar{n}$ cross section are shown in Fig. 3 (left). The statistical accuracy of the measurement is significantly improved compared with the previous SND measurement [14]. However the new SND result is lower than the previous one by about 30% at 1.9 GeV and by two times near 2 GeV. The main reasons are underestimated beam background and not quite correct MC simulation in the previous measurement. The systematic uncertainty on the cross section is estimated to be about 15%, mainly due to MC simulation.

The $e^+e^- \to n\bar{n}$ cross section depends on two form factors, magnetic and electric. From the measured cross section we determine the so-called effective form factor, which is shown in Fig. 3 (right) in comparison with with the BESIII measurement of the neutron form factor [17] above 2 GeV and the BABAR measurement of the proton form factor [16]. It is seen that the SND and BESIII results near 2 GeV are in agreement. The proton and neutron effective form factors are close to each other in the near-threshold region. The difference between them grows with increase of the energy.

The ratio of the form factors can be determined from the analysis of the antineutron polar angle distribution. The results of the fit to the angular distribution for the 2019 data set in three energy regions are listed in Table 2. Our preliminary results agree with the assumption that $|G_E/G_M| = 1$,

Table 2: Preliminary SND results on the $|G_E/G_M|$ ratio.

Energy range (GeV)	1.89–1.902	1.91–1.925	1.95–1.975
$\lvert G_E/G_M\rvert$	0.77 ± 0.27	1.34 ± 0.33	1.70 ± 0.53

but also do not contradict larger values $|G_E/G_M| \approx 1.4$–1.5 observed in the BABAR [16] and BESIII [18] experiments for the ratio of proton form factors near $E = 2$ GeV.

4. $e^+e^- \to \pi^+\pi^-\pi^0\gamma$ and $e^+e^- \to K^+K^-\pi^0\gamma$

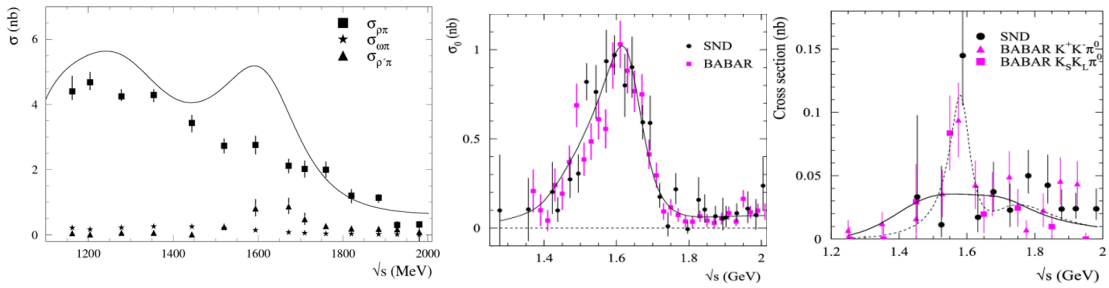

Figure 4: Left panel: The measured energy dependences of the cross sections for the intermediate states $\rho(770)\pi$, $\rho(1450)\pi$, and $\omega\pi^0$. The curve is the result of the VMD fit to the SND data on the total $e^+e^- \to \pi^+\pi^-\pi^0$ cross section. Middle panel: The $e^+e^- \to K^+K^-\pi^0$ cross section measured by SND (circles) compared with the BABAR [21] data (squares). The curve is the result of the VMD fit with the $\phi(1020)$ and $\phi(1680)$ resonances. Right panel: The $e^+e^- \to \phi\pi^0 \to K^+K^-\pi^0$ cross section measured by SND in comparison with the two BABAR measurements [21, 22]. The solid curve represents the VMD fit to the SND and BABAR data with the $\rho(1450)$ and $\rho(1700)$ resonances, while the dashed curves is the result of the same fit with free parameters of the first resonance.

.

These two processes are analyzed using data with an integrated luminosity of 35 pb^{-1} collected in 2011-2012. In the energy region 1.15–2.0 GeV we study the dynamics of the process $e^+e^- \to \pi^+\pi^-\pi^0$ [19]. The energy region is divided into 14 intervals. For each interval, the Dalitz plot distribution and $\pi^+\pi^-$ mass spectrum are fitted by the model containing a coherent sum of amplitudes for the three intermediate states: $\rho(770)\pi$, $\rho(1450)\pi$, and $\omega\pi^0$. The results of the fit in presented in Fig. 4 (left), where the fitted cross section for the intermediate states are shown together with the total $e^+e^- \to \pi^+\pi^-\pi^0$ cross section. It is seen that the cross section for $\rho(1450)\pi$ ($\sigma_{\rho'\pi}$) differs from zero in the region of the second maximum in the $e^+e^- \to \pi^+\pi^-\pi^0$ cross section, corresponding to the $\omega(1650)$ resonance. In the cross section for $\rho(770)\pi$ ($\sigma_{\rho\pi}$), the resonance structure near 1650 MeV is not seen. We conclude that the intermediate state $\rho(1450)\pi$ gives a significant contribution to the decay of $\omega(1650) \to \pi^+\pi^-\pi^0$, while the $\rho(770)\pi$ dominates in the $\omega(1420) \to \pi^+\pi^-\pi^0$ decay. The difference between the total cross section and the sum of the three cross sections for the intermediate states is due to interference.

The process $e^+e^- \to K^+K^-\pi^0$ below 2 GeV proceeds predominantly through the $K^*(892)^\pm K^\mp$ intermediate state, but the signal from the $\phi\pi^0$ intermediate state is also seen. The cross sections for the process $e^+e^- \to K^+K^-\pi^0$ (without $\phi\pi^0$) and $e^+e^- \to \phi\pi^0 \to K^+K^-\pi^0$ have been measured

separately [20]. The measured cross sections shown in Fig. 4 (middle and right) agree well with the previous measurements in the BABAR experiment [21, 22] and have comparable accuracy. In the narrow region near $\sqrt{s} = 1.58$ GeV all three existing measurements of the $e^+e^- \to \phi\pi^0$ cross section [see Fig. 4(right)] show excess over the model including known vector resonances. This excess can be interpreted as a contribution of the resonance with $M = 1585 \pm 15$ MeV and $\Gamma = 75 \pm 30$ MeV. Its significance is estimated to be about 3σ.

5. Radiative processes $e^+e^- \to \eta\pi^0\gamma$ and $e^+e^- \to \eta\eta\gamma$

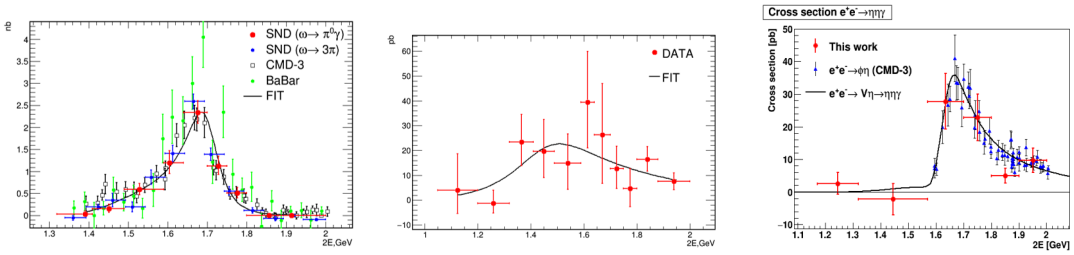

Figure 5: Left panel: The $e^+e^- \to \omega\eta$ cross section measured by SND in the $\eta\pi^0\gamma$ final state in comparison with the SND [24] and CMD-3 [25] measurements in the $\pi^+\pi^-\pi^0\eta$ final state. Middle panel: The non-$\omega\eta$ $e^+e^- \to \eta\pi^0\gamma$ cross section measured by SND. Right panel: The the $e^+e^- \to \eta\eta\gamma$ cross section measured by SND (circles) compared with the $e^+e^- \to \phi\eta$ cross section measured by CMD-3 in the decay mode $\phi \to K^+K^-$ [27] (triangles). The solid curve is the sum of the $e^+e^- \to \phi\eta$, $\rho\eta$ and $\omega\eta$ cross sections.

.

The processes $e^+e^- \to \eta\pi^0\gamma$ [23] and $e^+e^- \to \eta\eta\gamma$ [26] above 1.05 GeV have been measured for the first time. They have been studied in the five-photon final state.

In the process $e^+e^- \to \eta\pi^0\gamma$, there is a significant contribution of the $\omega\eta$ intermediate state, which is seen as a peak at ω mass in the $\pi^0\gamma$ mass distribution. The non-$\omega\eta$ signal is also observed. It may arise from the processes $e^+e^- \to a_0(1450)\gamma$ and $a_2(1320)\gamma$. Figure 5 (left) shows the measured $e^+e^- \to \omega\eta$ cross section in comparison with the SND and CMD-3 measurements in the decay mode $\omega \to 3\pi$, while Fig. 5 (middle) represents the first measurement of the non-$\omega\eta$ part of the $e^+e^- \to \eta\pi^0\gamma$ cross section.

The dominant intermediate state in the process $e^+e^- \to \eta\eta\gamma$ is $\phi\eta$. The measured cross section shown in Fig. 5 (right) is consistent with the CMD-3 result on $e^+e^- \to \phi\eta$ obtained in the decay mode $\phi \to K^+K^-$. The contribution from intermediate states other than $\phi\eta$ is not seen. The upper limits are set on a possible contribution of radiative intermediate states as $f_0(1500)\gamma$ or $f_2'(1525)\gamma$. In the energy range of the $\rho(1700)$ and $\phi(1680)$ resonances the limit is 11 pb at 90% confidence level.

Acknowledgments. This work is supported in part by the RFBR grants 20-02-00060 and 20-02-00347.

References

[1] M. N. Achasov *et al.*, Nucl. Instrum. Methods Phys. Res., Sect. A **598**, 31 (2009).

[2] V. M. Aulchenko *et al.*, Nucl. Instrum. Methods Phys. Res., Sect. A **598**, 102 (2009).

[3] A. Y. Barnyakov *et al.*, JINST **9**, C09023 (2014).

[4] V. M. Aulchenko *et al.*, Nucl. Instrum. Methods Phys. Res., Sect. A **598**, 340 (2009).

[5] A. Romanov *et al.*, in *Proceedings of Particle Accelerator Conference PAC 2013, Pasadena, CA USA, 2013*, p. 14.

[6] M. N. Achasov *et al.* (SND Collaboration), JHEP **01**, 113 (2021).

[7] M. N. Achasov and A. S. Kupich, JINST **12**, C06035 (2017).

[8] M. N. Achasov *et al.* (SND Collaboration), J. Exp. Theor. Phys. **103**, 380 (2006).

[9] M. Tanabashi *et al.* (Particle Data Group), Phys. Rev. D **98**, 010001 (2018).

[10] R.R. Akhmetshin *et al.* (CMD-2 Collaboration), Phys. Lett. B **648**, 28 (2007).

[11] J. P. Lees *et al.* (BaBar Collaboration), Phys. Rev. D **86**, 032013 (2012).

[12] A. Anastasi *et al.* (KLOE Collaboration), JHEP **03**, 173 (2018).

[13] A. Antonelli *et al.* (FENICE Collaboration), Nucl. Phys. B **517**, 3 (1998).

[14] M. N. Achasov *et al.* (SND Collaboration), Phys. Rev. D **90**, no. 11, 112007 (2014)

[15] M. N. Achasov *et al.*, JINST, **10**, T06002 (2015).

[16] J. P. Lees *et al.* (BaBar Collaboration), Phys. Rev. D **87**, 092005 (2013).

[17] M. Ablikim *et al.* (BESIII Collaboration), arXiv:2103.12486 [hep-ex].

[18] M. Ablikim *et al.* (BESIII Collaboration), Phys. Rev. Lett. **124**, 042001 (2020).

[19] M. N. Achasov *et al.* (SND Collaboration), Eur. Phys. J. C **80**, 993 (2020).

[20] M. N. Achasov *et al.* (SND Collaboration), Eur. Phys. J. C **80**, 1139 (2020).

[21] B. Aubert *et al.* (BABAR Collaboration), Phys. Rev. D **77**, 092002 (2008).

[22] J. P. Lees *et al.* (BABAR Collaboration), Phys. Rev. D **95**, 052001 (2017).

[23] M. N. Achasov *et al.* (SND Collaboration), Eur. Phys. J. C **80**, 1008 (2020).

[24] M. N. Achasov *et al.* (SND Collaboration), Phys. Rev. D **99**, 112004 (2019).

[25] R. R. Akhmetshin *et al.* (CMD-3 Collaboration), Phys. Lett. B **773**, 150 (2017).

[26] M. N. Achasov *et al.* (SND Collaboration), arXiv:2110.05845 [hep-ex].

[27] V. L. Ivanov *et al.* (CMD-3 Collaboration) Phys. Lett. B **798**, 134946 (2019).

PoS(EPS-HEP2021)404